

Insulator phases of Bose-Fermi mixtures induced by next-neighbor interactions between fermions

F. Gómez-Lozada,¹ R. Franco,¹ and J. Silva-Valencia^{1, 2, *}

¹Departamento de Física, Universidad Nacional de Colombia, A. A. 5997 Bogotá, Colombia.

²Department of Mechanical Engineering and Materials Science, University of Pittsburgh, Pittsburgh, PA, USA.

(Dated: September 12, 2023)

We study a one-dimensional mixture of two-color fermions and scalar bosons at the hard-core limit, focusing on the effect that the next-neighbor interaction between fermions has on the zero-temperature ground state of the system for different fillings of each carrier. Exploring the parameters of the problem, we observed that the non-local interaction modifies the well-known mixed and spin-selective Mott insulators, and we also found the emergence of three unusual insulating states with peculiar charge density wave orderings, a fully out-of-phase density of carriers for bosonic half-filling, an insulator with the same bosonic and fermionic fillings, and a different spin-selective insulator where the bosonic filling matches the density of one kind of fermion. Modern cold-atom setups correspond to the ideal experimental setting where these incommensurable insulators can be observed.

I. INTRODUCTION

Over the last few decades, the study of cold atoms has grown at a quick pace, to the point of being able to control the interactions and dynamics of many-body quantum systems to a great extent in so-called quantum simulators [1–4]. Of particular importance is the physics of the different insulators found in bosonic or fermionic systems, which have been detected and manipulated in these cold atom setups [5–10]. Taking a step further, one can wonder what happens when we deal with a mixture of both bosons and fermions. In fact, these systems have been studied for decades, with one of the first examples being the ${}^3\text{He}-{}^4\text{He}$ combination [11, 12]. Since then, there have been numerous experimental studies which deal with these types of mixtures, where the usual methodology is to use combinations of specific isotopes from the same or different atoms in order to produce disparate statistics between components [13–37]. Furthermore, controlling both the number of carriers from each species and the interactions between them has allowed finding novel and fascinating phenomena such as phase separation [38], a Bose-Fermi superfluid mixture [39], and even effective interactions between bosons mediated by fermions [40].

In order to perform a theoretical study of these mixtures, it is usual to describe fermions and bosons using the Hubbard model along with coupling terms that account for interspecies interactions. Within this framework, there have been abundant numerical and analytical studies, which has resulted in the prediction of diverse kinds of carriers' configurations, such as Luttinger liquids, charge density waves (CDW), and Mott insulators, among others [41–66]. Of particular interest for this research are the superfluid-insulator transitions, where it is well known that the insulator phases are characterized

by commensurable relations between the fixed fermionic ρ_F and bosonic densities ρ_B . Specifically, for a two-color fermion and scalar boson mixture with repulsive inter-species interactions, there is always one mixed Mott insulator characterized by the relation $\rho_B + \rho_F = n$ (n being an integer) and a spin-selective Mott insulator that follows $\rho_B + \rho_F^{\uparrow, (\downarrow)} = n$, which indicates that for a population imbalance this last insulator is divided in two [27, 67–71].

Non-local interactions are relevant in physics not only from a theoretical point of view, but also from an experimental one, where the effect of long-range interactions has recently been observed in diverse setups [72, 73]. Moreover, the next-neighbor interactions in bosonic or fermionic systems have enriched the ground-state phase diagram, allowing diverse configurations of the carriers. For instance, taking into account non-local interactions in a bosonic system has led to the emergence of exotic phases such as supersolid, Haldane, and solitonic ones, and furthermore the charge-density wave (CDW) phase for integer and half-integer densities [74–78]. On the other hand, the one-dimensional phase diagram of fermions under local and non-local interactions is well-known for half filling, although it is controversial and little studied for other fillings [79–86]. At half filling, a charge density wave phase emerges when the long-range interaction prevails over the on-site one and a spin density wave when the opposite happens. In addition, other phases appear, such as a bond density wave when both interactions are of the same order, a phase separation for attractive interactions, and certain superconductor phases, both singlet and triplet.

Despite the interesting physics generated by the non-local interactions, there are only a few studies where this effect is considered for a Bose-Fermi mixture, with one example being an investigation with polarized fermions [87]. Hence we proposed an exploration of the extended Bose-Fermi Hubbard model with two-color fermions and scalar bosons at the hard core limit, including next-neighbor interactions between fermions. As

* jsilvav@unal.edu.co

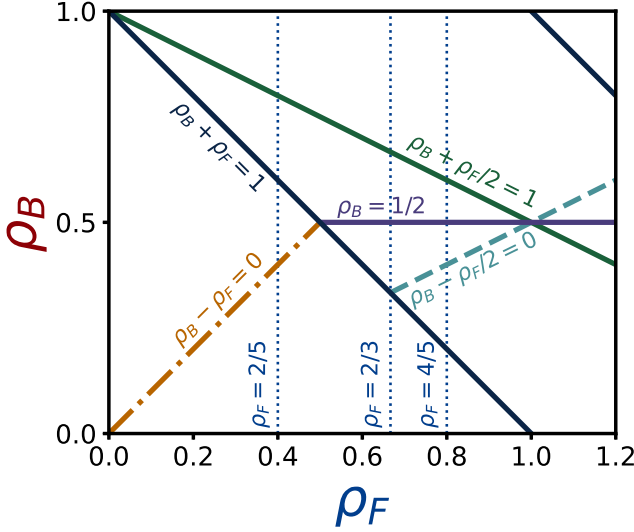


FIG. 1. Phase diagram of the possible insulator phases that can appear in a balanced Bose-Fermi mixture. This contains the well-known mixed Mott insulator $\rho_B + \rho_F = 1$ (dark blue line) and the spin-selective Mott insulator $\rho_B + \rho_F/2 = 1$ (dark green line), while also including the three phases found: the immiscible CDW $\rho_B = 1/2$ (purple line), the mixed CDW $\rho_B - \rho_F = 0$ (brown line) and the spin-selective CDW $\rho_B - \rho_F/2 = 0$ (light green line). The vertical lines signal special densities that are related to Fig. 2, 4, and 6. The diagram includes only part of the range $\rho_F > 1$, since this region corresponds to a reflection of the $\rho_F < 1$ diagram thanks to the particle-hole symmetry of the Hamiltonian.

a result, we were able to obtain the phase diagram of Fig. 1, which summarizes the different insulator phases that can appear at a given filling. The latter contains the well-known mixed and spin-selective Mott insulators, as well as three unusual incommensurable insulators that appear when taking into account the next-neighbor interaction between fermions. One of them corresponds to an immiscible charge density wave located at $\rho_B = 1/2$, where both fermions and bosons are in completely unsynchronized CDW phases. The other two correspond to coupled global and local charge density wave orderings, which fulfill the relations $\rho_B - \rho_F = 0$ and $\rho_B - \rho_F^{\uparrow,(\downarrow)} = 0$, the last being a spin-selective phase analog to its Mott counterpart.

Therefore, the main objective of this article is to study the conditions under which these incommensurable insulators appear, as well as to expose the main properties that characterize their structure. In order to achieve this, in Sec. II we first present the extended Bose-Fermi Hubbard model to be used, along with a discussion of our numerical techniques, which are matrix product states (MPS) optimization algorithms for finding the ground state. The main results are found in Sec. III, where we perform the analysis of Fig. 1 by choosing three representative fermionic densities given by $\rho_F \in \{2/5, 2/3, 4/5\}$, each of which shows a particular incommensurable in-

sulator along with the principal characteristics from the phase diagram. Accordingly, in each subsection we study the corresponding $\rho_B - \mu_B$ and $\mu_B - V_{FF}$ diagrams in conjunction with multiple density profiles as a means of analyzing the properties of the different incompressible phases and their dependence on the fermionic next-neighbor interaction, with a particular focus on the incommensurable ones. Finally, in Sec. IV we give some final remarks and future perspectives for research.

II. MODEL

A mixture of bosonic and fermionic atoms is commonly described by taking into account a local interaction term between bosons and fermions plus a Hubbard-type Hamiltonian for each species, leading to the following expression:

$$\hat{H} = \hat{H}_B + \hat{H}_F + \hat{H}_{BF}, \quad (1)$$

$$\hat{H}_B = -t_B \sum_{\langle i,j \rangle} \left(\hat{b}_i^\dagger \hat{b}_j + \text{h.c.} \right) + \frac{U_{BB}}{2} \sum_i \hat{n}_i^B (\hat{n}_i^B - 1), \quad (2)$$

$$\begin{aligned} \hat{H}_F = -t_F \sum_{\langle i,j \rangle, \sigma} \left(\hat{f}_{\sigma,i}^\dagger \hat{f}_{\sigma,j} + \text{h.c.} \right) + U_{FF} \sum_i \hat{n}_{\uparrow,i}^F \hat{n}_{\downarrow,i}^F \\ + V_{FF} \sum_{\langle i,j \rangle} \hat{n}_i^F \hat{n}_j^F, \end{aligned} \quad (3)$$

$$\hat{H}_{BF} = U_{BF} \sum_i \hat{n}_i^B \hat{n}_i^F, \quad (4)$$

which is defined on a one-dimensional chain of length L with open boundary conditions for the numerical efficiency. In the above Hamiltonian $\hat{b}_i^\dagger, \hat{b}_i$ ($\hat{f}_{\sigma,i}^\dagger, \hat{f}_{\sigma,i}$) are the creator and annihilator boson (fermion with spin $\sigma \in \{\uparrow, \downarrow\}$) operators at the i -th site with their corresponding number operators $\hat{n}_i^B = \hat{b}_i^\dagger \hat{b}_i$, $\hat{n}_{\sigma,i}^F = \hat{f}_{\sigma,i}^\dagger \hat{f}_{\sigma,i}$ and $\hat{n}_i^F = \hat{n}_{\uparrow,i}^F + \hat{n}_{\downarrow,i}^F$. The hopping integral for bosons (fermions) is t_B (t_F), where $\langle i, j \rangle$ indicates next-neighbor pairs, and U_{BB} (U_{FF}) is the intensity of the local boson-boson (fermion-fermion) interaction, while the interspecies interaction is modulated by U_{BF} . Knowing that next-neighbor interactions are relevant, we consider them between fermions, and their strength is quantified by V_{FF} .

Additionally, the previous Hamiltonian admits a set of appropriate Abelian quantum numbers given by the boson number N_B and the fermion number N_F^σ with spin $\sigma \in \{\uparrow, \downarrow\}$. From them we define useful quantities for the rest of the study, such as the total fermion number $N_F = N_F^\uparrow + N_F^\downarrow$, the global boson density $\rho_B = N_B/L$, and the global fermion densities $\rho_F^\sigma = N_F^\sigma/L$, and $\rho_F = N_F/L$. We also define $I = |\rho_F^\uparrow - \rho_F^\downarrow|/\rho_F$ as the imbalance of spin population.

Since the local Hilbert space for bosons is computationally intractable, we perform a cut in this local dimension

by assuming the hard core limit, which implies that there can be at most one boson per site. The latter sets a local basis of dimension 8 given by all of the combinations $|n_B\rangle|n_{F\uparrow}\rangle|n_{F\downarrow}\rangle$ where each carrier number is either 0 or 1. Also, the hard core limit is equivalent to assuming an infinite on-site boson interaction ($U_{BB} \rightarrow \infty$) and hence we do not take this process into account for the rest of the paper. In order to further simplify our analysis, we suppose that $t_B = t_F = 1$, while also establishing our energy scale; therefore, all quantities are measured with respect to them. This last assumption is supported by the fact that these mixtures are usually constructed with isotopes of the same atom, for example with the ${}^6\text{Li}$ - ${}^7\text{Li}$ [88] or ${}^{171}\text{Yb}$ - ${}^{174}\text{Yb}$ [89] combinations.

For the purpose of achieving insight into the physics of this model, we perform a ground-state energy search for a given set of particle fillings $E(N_B, N_F^\uparrow, N_F^\downarrow)$ and different interaction strengths, using a density matrix renormalization group (DMRG) algorithm based on the MPS language [90] with the help of the TeNPy library [91]. We set a maximum truncation error of 10^{-14} , which varies with the bond dimension between sweeps and sites of the chain. On the other hand, since the addition of next-neighbor interactions gives rise to a need for extra degrees of entanglement, we employ a sweep-dependent bond dimension which starts at a given value between 500 and 1000 and increases each 10 sweeps by 100. The optimization code stops when the energy (entropy) error goes beyond the 10^{-5} (10^{-3}) limit.

III. EXPLORATION OF THE PHASE DIAGRAM

We focus our analysis of the phase diagram from Fig. 1 on three essential fermionic densities given by $\rho_F \in \{2/5, 2/3, 4/5\}$, showing for each of them the emergence of an unknown insulator, along with a discussion on how the next-neighbor interactions between fermions affects the already well-known insulator phases. For these investigations, we fix the on-site interactions at $U_{FF} = 4$ and $U_{BF} = 6$, while we choose a next-neighbor interaction, which will be within the range $0 \leq V_{FF} \leq 6$. In order to detect the insulator phases, we measure the bosonic chemical potential $\mu_B(N_B, N_F^\uparrow, N_F^\downarrow) = E(N_B, N_F^\uparrow, N_F^\downarrow) - E(N_B - 1, N_F^\uparrow, N_F^\downarrow)$ while varying the bosonic density from zero to one and look for plateaus in the curve of $\rho_B - \mu_B$, which indicates the presence of an insulator, along with an extrapolation to the thermodynamic limit in order to determine the corresponding gap $\Delta_B = \mu_B(N_B + 1, N_F^\uparrow, N_F^\downarrow) - \mu_B(N_B, N_F^\uparrow, N_F^\downarrow)$.

A. Two thirds fermionic filling ($\rho_F = 2/3$)

In Fig. 2(a), we show the bosonic density ρ_B as a function of the bosonic chemical potential μ_B for $V_{FF} = 0$ (black open squares) and $V_{FF} = 2$ (red filled circles). The inset shows the charge gap Δ_B as a function of the system size L for each plateau found for $V_{FF} = 2$.

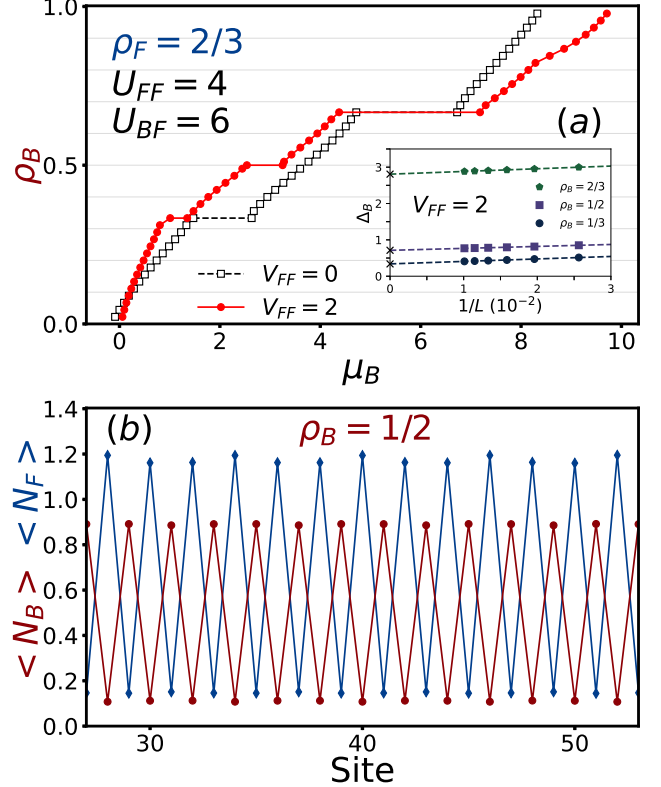


FIG. 2. (a) Bosonic density ρ_B vs bosonic chemical potential μ_B at the thermodynamic limit for a balanced mixture with a fermionic density $\rho_F = 2/3$ and local interactions $U_{FF} = 4$, and $U_{BF} = 6$. Here we compare the behavior with and without next-neighbor interaction between fermions, using $V_{FF} \in \{0, 2\}$. The inset shows the charge gap Δ_B as a function of the system size L for each plateau found for $V_{FF} = 2$. In (b), we show the density profile for bosons $\langle N_B \rangle$ and fermions $\langle N_F \rangle$ at the plateau with $\rho_B = 1/2$ found in (a). The points correspond to DMRG results, and the lines are visual guides.

For the turned-off next-neighbor interaction, in the majority of the graph we found a monotonous increase in μ_B as we continuously add bosons to the system, which corresponds to the presence of superfluid phases, since they have non-zero compressibility. In particular, this behavior finds its exceptions at $\rho_B \in \{1/3, 2/3\}$ where the graph is discontinuous; that is, we found incompressible phases. Each plateau in the $\rho_B - \mu_B$ curve represents the presence of an insulator state, where we denote its charge gap Δ_B as the length of the plateau. At $\rho_B = 1/3$ we found, with a charge gap $\Delta_B^{\rho_B=1/3} = 1.16$, the well-known mixed Mott insulator in which the interplay between commensurability of both bosons and fermions and their mutual interaction generate the presence of an incompressible phase. On the other hand, for $\rho_B = 2/3$, a plateau with a charge gap of $\Delta_B^{\rho_B=2/3} = 2.01$ appears, which we identify as a spin-selective Mott insulator, which has an analog behavior as does the previous

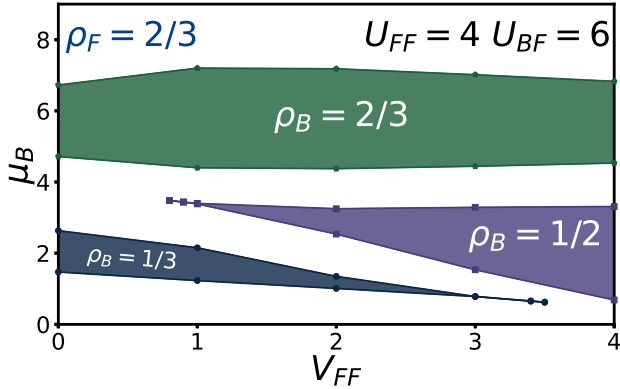


FIG. 3. Phase diagram of the bosonic chemical potential μ_B vs. next-neighbor fermion interaction magnitude V_{FF} at the thermodynamic limit for a fermionic density $\rho_F = 2/3$ without spin imbalance and local interactions $U_{FF} = 4$ and $U_{BF} = 6$. Here we show the evolution of the respective charge gaps from each insulator phase shown in Fig. 2(a). The points are extrapolations of the chemical potential to the thermodynamic limit, and the lines are visual guides.

phase, but instead the association is between bosons and only one type of fermion (spin up or down). These insulator phases are already known in the literature [27, 67–71] and follow the relations $\rho_B + \rho_F = 1$ for the mixed Mott insulator and $\rho_B + \rho_F/2 = 1$ for the spin-selective Mott insulator in a balanced Bose-Fermi mixture.

After turning on the next-neighbor interaction, we found ourselves in a similar context, where most of the graph is in a superfluid phase. We still observe both previously mentioned insulators, but now their charge gaps change. For the mixed Mott insulator, we found that the gap decreases to $\Delta_B^{\rho_B=1/3} = 0.34$, less than a third of its original value. In this case, because $\rho_F > 1/2$ the fermions are not able to leave empty spaces between each pair of them in their commensurable organization with the bosons. This generates an effective pressure produced by the next-neighbor interaction that makes the insulator less stable as we increase V_{FF} . On the other hand, the spin-selective Mott insulator slightly increases its gap to $\Delta_B^{\rho_B=2/3} = 2.81$, showing that this phase benefits from the non-local fermion interaction. Of course, since only half of the fermions are coupled to the bosons ($\rho_F^{\uparrow, \downarrow} = 1/3$) and this is less than one half, both the commensurable and the next-neighbor interaction orderings collaborate, increasing the insulator stability, and hence its charge gap.

On observing Fig. 2(a) for $V_{FF} = 2$, we notice that an additional incompressible phase at $\rho_B = 1/2$ emerges with a charge gap of $\Delta_B^{\rho_B=1/2} = 0.71$. In order to characterize this mysterious insulator, in Fig. 2(b) we show the corresponding bosonic and fermionic density profiles. Since the fermions repel each other, the optimal configuration is to leave space between them, which produces the characteristic oscillating pattern from the

CDW phase. Moreover, since the bosons also interact with the fermions locally, they locate themselves between them, which generates another CDW ordering. Since the patterns are out of phase with each other, we call this insulator an immiscible CDW. This curious insulator always appears at $\rho_B = 1/2$ (see Fig. 1), since only for this bosonic density is the CDW structure stable for both species. That is, if there were more bosons, they could not fit between the fermions, and if there were fewer bosons, the fermions could flow freely through the spaces left behind by the missing bosons, removing the insulator condition. This last fact shows that this phase represents the first example of an incommensurable insulator in the Bose-Fermi mixture model, product of non-local interactions. Even then, this phase does not appear for every fermionic density. Specifically, for $\rho_F < 1/2$, the system does not have enough fermions to build the sub-lattice for the CDW ordering. This is independent of the spin population imbalance, since the CDW ordering can be built with different types of fermions. On the other hand, for $I \neq 0$ there is another limitation. Consider the case where ρ_F^{\uparrow} or ρ_F^{\downarrow} are larger than half filling; then all of the fermions with the corresponding spin do not fit in the CDW ordering, and hence it is not possible to construct the insulating phase. Both restrictions can be summarized with the mathematical condition that the immiscible CDW phase only appears for $1/2 \leq \rho_F \leq 1/(1+I)$.

The immiscible CDW phase of Bose-Fermi mixtures has already been reported in the literature for spin-polarized fermions [87], which corresponds to $I = 1$, and according to this study there is only one possible density combination in which the insulator can appear, namely $\rho_F = \rho_B = 1/2$. With this, we have shown that the specific case for spin-polarized systems admits a more general family of density combinations in the two-color fermion model.

Let's analyze what happens when we vary the next-neighbor interaction. In order to do this, in Fig. 3 we show the evolution of the respective charge gaps from each phase as we increase the value of the next-neighbor interaction from $V_{FF} = 0$ to $V_{FF} = 4$. First, we observe that for the immiscible CDW phase at $\rho_B = 1/2$ there exists a critical value $V_{FF}^{*\rho_B=1/2} = 0.85 \pm 0.05$ from which the insulator appears; to put it another way, for $V_{FF} \geq V_{FF}^{*\rho_B=1/2}$ we find a non-zero charge gap associated with this incompressible phase. Moreover, this charge gap increases with V_{FF} , since for a bigger next-neighbor interaction the stability of the CDW ordering improves. On the other hand, for the mixed Mott insulator at $\rho_B = 1/3$, we see that the charge gap decreases monotonously until it vanishes at a critical value of $V_{FF}^{*\rho_B=1/3} = 3.45 \pm 0.05$, since the commensurable condition is incompatible with high V_{FF} values. For the spin-selective Mott insulator, even though we observed an initial increase in its charge gap, here we find that after a certain value the gap starts to decrease monotonously. This behavior is persistent until the charge gap vanishes at a very high V_{FF} value, not shown here. Al-

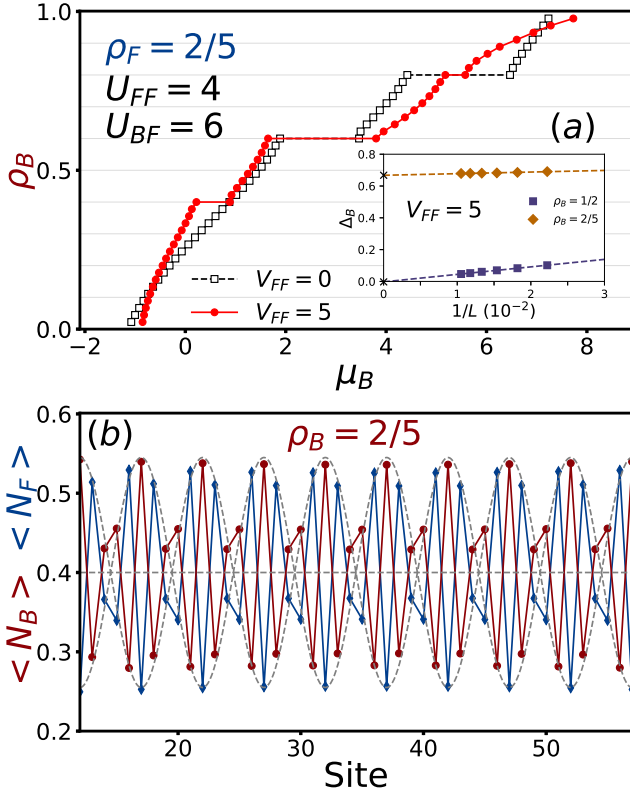


FIG. 4. (a) Progress of the bosonic chemical potential of a balanced mixture as the number of bosons grows for a fermionic density $\rho_F = 2/5$ ($\rho_B - \mu_B$ curve). Here, we consider that $U_{FF} = 4$, $U_{BF} = 6$, and compare the behavior with and without next-neighbor interaction between fermions, using $V_{FF} \in \{0, 5\}$. The inset shows the charge gap Δ_B as a function of the system size L for $V_{FF} = 5$ at $\rho_B \in \{2/5, 1/2\}$. In (b), we show the density profile for bosons $\langle N_B \rangle$ and fermions $\langle N_F \rangle$ at the plateau with $\rho_B = 2/5$ found in (a), along with dashed lines that only act as visual guides. The latter density profiles were evaluated with periodic boundary conditions. The lines are visual guides, while the points correspond to DMRG results.

though the commensurable and CDW orderings work together for the coupled fermions in the spin-selective Mott insulator, the rest of them are in a superfluid phase [70, 71]; hence these free fermions, together with the enhanced next-neighbor interaction, destabilize the insulator phase, which then decreases the charge gap to the point of erasing it completely.

B. Two fifths fermionic filling ($\rho_F = 2/5$)

From this point on, we will explore a lower fermionic density, $\rho_F = 2/5$, in a manner similar to that of section Sec. III A; therefore, we plot the $\rho_B - \mu_B$ graph for $\rho_F = 2/5$ in Fig. 4(a), but in this case the next-neighbor interaction is modulated between $V_{FF} = 0$ and 5. Without non-local interactions (black open squares), we ob-

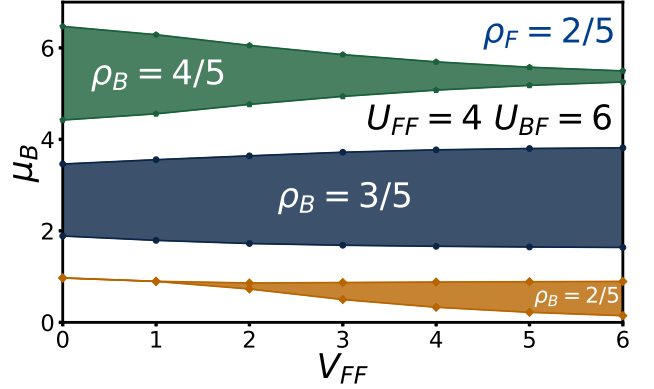


FIG. 5. Evolution of the insulating lobes with the next-neighbor fermion interaction for a Bose-Fermi mixture with a fermionic density $\rho_F = 2/5$ and local interactions $U_{FF} = 4$ and $U_{BF} = 6$. The white regions are related to superfluid states, while the colored ones correspond to the insulators shown in Fig. 4(a). The dots correspond to extrapolations from DMRG results, while the lines are visual guides.

tain the already expected plateaus related to the mixed and spin-selective Mott insulators at $\rho_B \in \{3/5, 4/5\}$ with gaps $\Delta_B^{\rho_B=3/5} = 1.57$ and $\Delta_B^{\rho_B=4/5} = 2.05$. In the presence of next-neighbor interactions (red filled circles), we can predict certain behavior based on the previous discussion. Since we find ourselves in a region that fulfills $\rho_F < 1/2$, according to Fig. 1 we do not observe a plateau associated with the immiscible CDW, which is further emphasized by considering the thermodynamic limit extrapolation shown in the inset of Fig. 4(a). Instead, the mixed and spin-selective Mott insulators still emerge, but in this case the first one increases its charge gap to $\Delta_B^{\rho_B=3/5} = 2.15$, while the latter decreases its gap to $\Delta_B^{\rho_B=4/5} = 0.40$ when the non-local interaction is turned on, which is contrary to what happens in Fig. 2. For the mixed Mott insulator, we have a fermionic density lower than half filling, so in the commensurable ordering with the bosons we can locate the fermions with spacing between them, hence avoiding the effective pressure that the next-neighbor fermion interaction can produce and instead enhancing the stability of the insulating phase. For the spin-selective Mott insulator, we associate the charge gap decrease with the instability produced by the free fermions not coupled with the bosons and enhanced by the next-neighbor interaction. When we look at the evolution of the charge gaps from both previously mentioned insulators as we increase V_{FF} , as shown in Fig. 5, we observe the same behavior; that is, the gap of the mixed Mott insulator grows with higher next-neighbor interactions and that of the spin-selective Mott insulator decreases.

Furthermore, because of the non-local interaction, an unusual incompressible phase emerges at $\rho_B = 2/5$, with a charge gap of $\Delta_B^{\rho_B=2/5} = 0.67$ and whose thermodynamic limit extrapolation is shown in the inset of

Fig. 4(a). This particular insulator fulfills the relation $\rho_B - \rho_F = 0$, as shown in Fig. 1, which means, among other things, that except for half filling it corresponds to an incommensurable phase. For the sake of getting insight into this particular insulator, we take a look at the respective boson and fermion density profiles shown in Fig. 4(b), where we recognize two sets of CDW orderings: a global one, which encloses both density profiles and a local CDW order analog to the immiscible CDW insulator. Here the global order has a periodicity of five sites imposed by the mutual density $\rho_B = \rho_F = 2/5$, while the local order always has a period of two sites characteristic of a typical CDW phase. The latter behavior was checked for different fermionic density values from the respective phase line of Fig. 1; hence it corresponds to a key characteristic of the phase, and because of that we will denote it a mixed CDW insulator. It is important to note that the previously mentioned density profiles were calculated with periodic boundary conditions, since with the usual open conditions a finite-size effect appears that enlarges the density profiles as we get closer to the boundaries and which does not allow correctly see the oscillating pattern that characterizes this insulator.

The balance of the two densities and the necessity of the next-neighbor interaction in order that the mixed CDW insulator appear suggests that its incompressible nature comes from the emergence of Bose-Fermi composites that have effective repulsive interactions between them, which generates the stability of the insulator. In other words, even if all of the carriers repel each other, locally or non-locally, they can still find a configuration where in they create interspecies pairs through quantum fluctuations. They can, at the cost of the internal repulsion inside them, minimize the long-range interaction between composites, thus generating an incompressible structure. This picture allows us to explain some aspects of the insulator. First, since the possibility of creating these Bose-Fermi composites lies in having sufficient space to separately locate each carrier, because of the repulsive interactions, the incompressible phase can only appear for $\rho_B + \rho_F \leq 1$, which is also a spin-independent condition. The limit case when $\rho_B + \rho_F = 1$ corresponds to the mutual half-filling situation $\rho_B = \rho_F = 1/2$ where both orderings attain a two-site periodicity, turning into the immiscible CDW insulator. Additionally, in Fig. 5 we find that the charge gap of the mixed CDW increases as V_{FF} grows, which shows that with a higher non-local interaction, the stability of the insulator improves through an increase in the effective repulsion between Bose-Fermi composites, which appears to be greater than the change in the pressure inside the pairing structure. We also believe that the incompressible phase appears right after introducing the non-local interaction between fermions, or to be more specific for $V_{FF} > 0$, but this assertion requires a more detailed study, since the calculation of the charge gap near zero next-neighbor interaction is unstable, probably because we are close to the critical value. The latter could be done with a bosonization method in

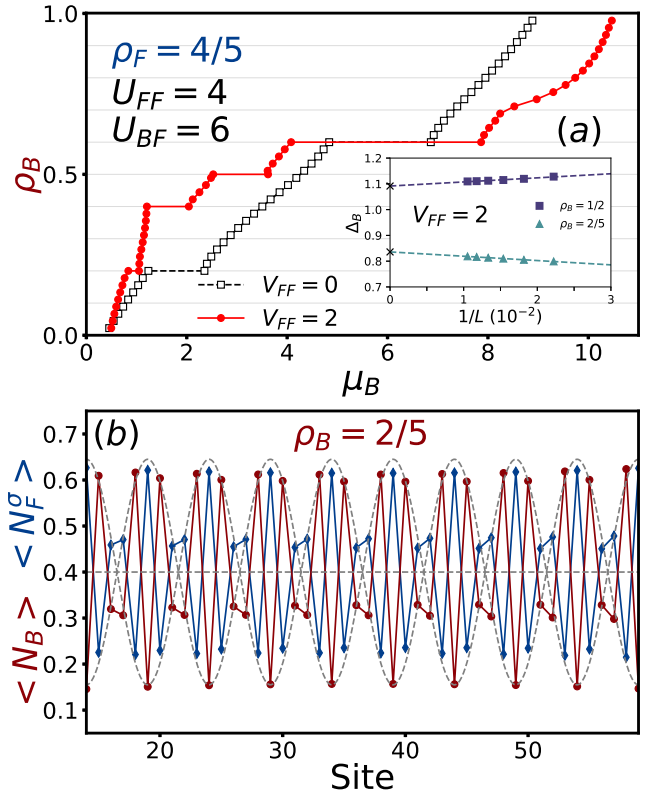


FIG. 6. Bosonic density ρ_B vs bosonic chemical potential μ_B at the thermodynamic limit for a fermionic density $\rho_F = 4/5$. The local repulsion couplings are $U_{FF} = 4$, and $U_{BF} = 6$, and we compare the behavior with and without next-neighbor interaction between fermions using $V_{FF} \in \{0, 2\}$. The inset shows the charge gap Δ_B as a function of the inverse of the system size L for $V_{FF} = 2$ at $\rho_B \in \{2/5, 1/2\}$. In (b), we show the density profile for bosons $\langle N_B \rangle$ and one color of fermions $\langle N_F^\sigma \rangle$ with $\sigma \in \{\uparrow, \downarrow\}$ at the plateau with $\rho_B = 2/5$ found in (a), along with dashed lines that only act as visual guides. The latter density profiles were evaluated with periodic boundary conditions. The points correspond to DMRG results and the lines are visual guides.

order to more precisely determine the nature of the phase transition, but this exceeds the scope of this paper.

C. Four fifths fermionic filling ($\rho_F = 4/5$)

As can be seen in Fig. 1, there is an unexplored region; therefore, we fix the fermionic density at $\rho_F = 4/5$ and calculate the bosonic chemical potential as the number of bosons grows, which is displayed in Fig. 6(a). Also, we follow the evolution of the respective charge gaps from each plateau as we vary the next-neighbor interaction according to $0 \leq V_{FF} \leq 4$ in Fig. 7. In the case of null next-neighbor interaction between fermions, we find the expected mixed and spin-selective Mott insulator plateaus at $\rho_B = \{1/5, 3/5\}$ with charge gaps

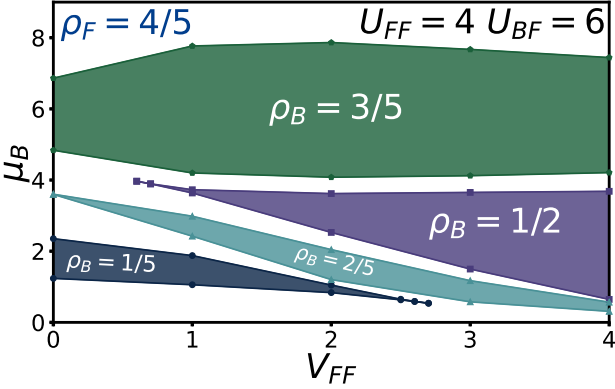


FIG. 7. Phase diagram of the bosonic chemical potential μ_B vs next-neighbor fermion interaction magnitude V_{FF} at the thermodynamic limit for a fermionic density $\rho_F = 4/5$ without spin imbalance and local interactions $U_{FF} = 4$ and $U_{BF} = 6$. The colored regions exhibit the evolution of the insulator states shown in Fig. 6(a), which are surrounded by superfluid regions. The dots correspond to extrapolations from DMRG results, while the lines are visual guides.

of $\Delta_B^{\rho_B=1/5} = 1.12$ and $\Delta_B^{\rho_B=3/5} = 2.02$. By including the non-local interaction, the immiscible CDW insulator predicted in Sec. III A emerges with a non-zero charge gap for next-neighbor interactions higher than the critical value $V_{FF}^{*, \rho_B=1/2} = 0.65 \pm 0.05$ (see Fig. 7). Then, as we increase V_{FF} we observe that the charge gap from the immiscible CDW insulator also increases monotonously, with the specific value of $\Delta_B^{\rho_B=1/2} = 1.09$ for $V_{FF} = 2$ corresponding to Fig. 6(a). On the other hand, in the presence of non-zero next-neighbor interactions the mixed Mott insulator decreases its charge gap to $\Delta_B^{\rho_B=1/5} = 0.21$ for $V_{FF} = 2$ as a consequence of the incompatibility between the commensurate ordering of bosons and fermions and the induced CDW ordering of the next-neighbor interactions. The latter continues as we increase V_{FF} until the corresponding plateau vanishes at $V_{FF}^{*, \rho_B=1/5} = 2.65 \pm 0.05$ (see Fig. 7). In the case of the spin-selective Mott insulator, its charge gap increases to $\Delta_B^{\rho_B=3/5} = 3.75$ for $V_{FF} = 2$, but as the next-neighbor interaction grows further, the gap starts to decrease, which is expected, since the free fermions of the spin-selective phase can more greatly disturb the insulating structure with higher V_{FF} values, hence reducing its stability. All of these scenarios are akin to the results found in Sec. III A for the three corresponding insulators, since between $\rho_F = 2/3$ and $\rho_F = 4/5$ there are no particular changes in their behavior.

Nevertheless, we do find a peculiar plateau, not seen in previous sections, when we turn on the next-neighbor interaction, which is located at $\rho_B = 2/5$ and has a charge gap of $\Delta_B^{\rho_B=2/5} = 0.83$. This particular incompressible phase appears when the density of the bosons equals half the density of the fermions; that is, $\rho_B - \rho_F/2 = 0$ and thus corresponds to an incommensurable insulator. As a

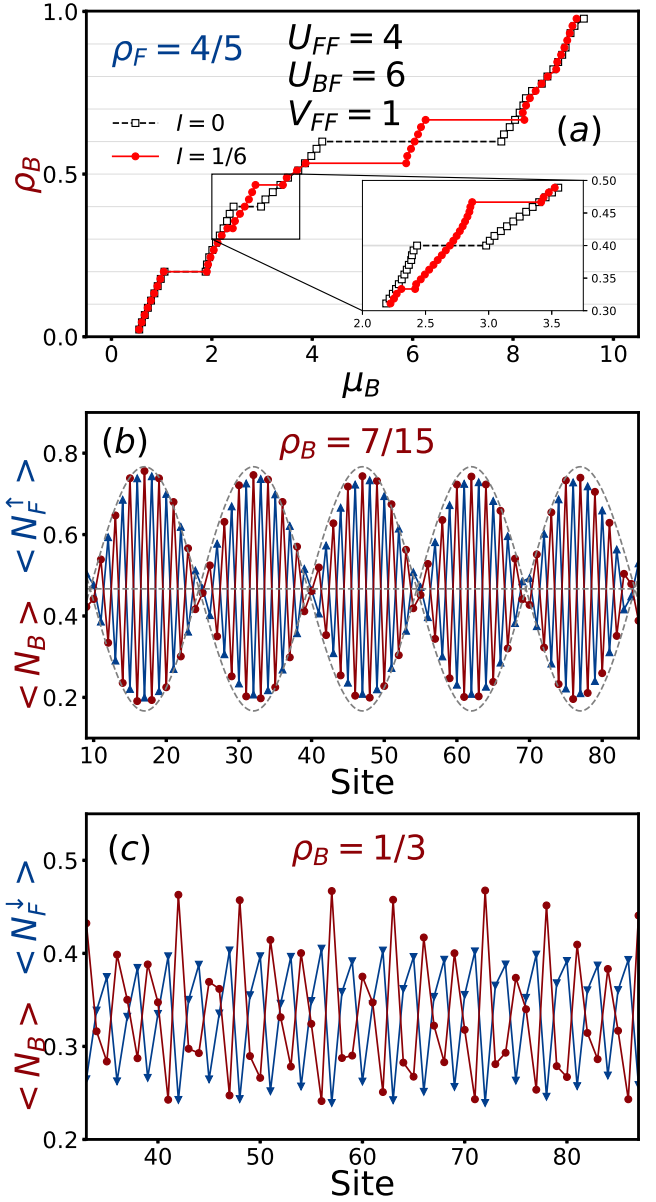


FIG. 8. Bosonic density ρ_B vs bosonic chemical potential μ_B at the thermodynamic limit for a fermionic density $\rho_F = 4/5$, local interactions $U_{FF} = 4$, $U_{BF} = 6$, and next-neighbor interaction $V_{FF} = 1$. Here we compare the behavior with and without spin imbalance using $I \in \{0, 1/6\}$. The inset shows a close-up of the region where a spin-selective insulator splits because of the non-zero spin population imbalance. In (b) and (c) we show the density profile for bosons $\langle N_B \rangle$ and fermions $\langle N_{F\uparrow(\downarrow)} \rangle$ at the plateaus with $\rho_B = 7/15$ and $\rho_B = 1/3$, respectively, found in (a), along with corresponding dashed lines that only act as visual guides. Both density profiles were evaluated with periodic boundary conditions. The lines are visual guides, while the points correspond to DMRG results.

means to shed light on its nature, in Fig. 6(b) we show its corresponding boson and fermion density profiles, where we can see the combination of a global oscillation and

a local CDW ordering previously observed in Fig. 4(b), but in this case the synchronization is between bosons and only one kind of fermion. This fact inspires us to explore the behavior of the system at the given fermionic density as we consider non-zero spin population imbalance. Therefore, in Fig. 8(a) we show the $\rho_B - \mu_B$ graph for $\rho_F = 4/5$ with a next-neighbor interaction of $V_{FF} = 1$ and different cases of spin-imbalance given by $I = 0$ and $I = 1/6$. Without spin imbalance (black open squares), we observe the expected plateaus corresponding to the mixed Mott insulator with gap $\Delta_B^{\rho_B=1/5} = 0.82$, the spin-selective Mott insulator with gap $\Delta_B^{\rho_B=3/5} = 3.57$, and the previously found incommensurable insulator with a gap of $\Delta_B^{\rho_B=2/5} = 0.56$. We do not find the immiscible CDW plateau, not because there is none, but because its charge gap has a small value of $\Delta_B^{\rho_B=1/2} = 0.09$, which is difficult to see at this scale. Nevertheless, this is not a problem, since we are currently focusing on the unfamiliar insulator (at $\rho_B = 2/5$) from this section.

After increasing the spin population imbalance to $I = 1/6$, we find that the charge gap of the mixed Mott insulator barely changes to $\Delta_B^{\rho_B=1/5} = 0.86$, while the spin-selective Mott phase splits into two plateaus at $\rho_B \in \{8/15, 2/3\}$ with corresponding charge gaps of $\Delta_B^{\rho_B=8/15} = 2.00$ and $\Delta_B^{\rho_B=2/3} = 1.97$. On top of that, we notice that the unfamiliar incommensurable insulator (at $\rho_B = 2/5$) also splits into two incompressible phases at $\rho_B \in \{1/3, 7/15\}$ with charge gaps of $\Delta_B^{\rho_B=1/3} = 0.11$ and $\Delta_B^{\rho_B=7/15} = 0.54$, which is further emphasized by the inset in Fig. 8(a). The latter indicates that this phase corresponds to a spin-selective insulator. Furthermore, by observing the density profiles for each plateau in Fig. 8(b), we once more recognize the characteristic behavior of the mixed CDW for $\rho_B = 7/15$, while the second profile for $\rho_B = 1/3$ does not have a clear structure. All of these previous findings express the fact that, analogous to the mixed CDW, a set of Bose-Fermi composites appears that generates the incompressible nature of the phase, but for this case the pairing is only between the bosons and the fermions with the corresponding spin, while the rest remain free in the system. So we call this a spin-selective CDW insulator. If this is true, why do we not see the characteristic oscillating structure in the density profile for $\rho_B = 1/3$? So in this case, the insulator has a high number of free fermions that damp out the incompressible structure of the insulator, compared to the plateau at $\rho_B = 7/15$, for which the number of uncoupled fermions is lower, and hence the ordering is more stable. This is further emphasized by the imbalance between the charge gaps of the two plateaus, given that the insulator at $\rho_B = 7/15$ has a gap five times larger than the one at $\rho_B = 1/3$, in contrast to the spin-selective Mott insulator, for which the two plateaus have balanced charge gaps.

The latter explains the behavior of the charge gap as we vary the next-neighbor interaction shown in Fig. 7. Then, on increasing V_{FF} from zero, the Bose-Fermi com-

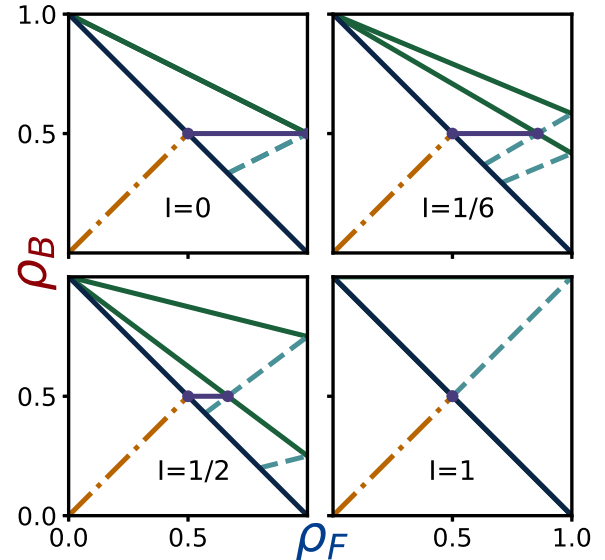


FIG. 9. Phase diagram of the possible insulator phases that can appear in a balanced Bose-Fermi mixture for different values of the spin population imbalance $I \in \{0, 1/6, 1/2, 1\}$. The phases correspond to the mixed Mott (dark blue line), mixed CDW (brown line), spin-selective Mott (dark green line), spin-selective CDW (light green line), and immiscible CDW (purple line) insulators.

posites start to appear, but since we have stronger next-neighbor interaction, the free fermions can perturb the paired structure until their stability starts to slowly decrease, and hence their gaps. Here we also believe that this incompressible phase appears for all $V_{FF} > 0$, like the mixed CDW insulator, but because of the instability of the charge gap calculation near this point we do not delve further into this discussion. On the other hand, this particular spin-selective phase appears only for $\rho_B + \rho_F \geq 1$, since in this region the chain gets saturated with all of the carriers, which forces the coupling to only contain one type of fermion and not both, in contrast to what happens with the mixed CDW. This condition is also independent of the spin population imbalance, since it only deals with the complete fermionic and bosonic densities.

D. Phase diagram for non-zero spin population imbalance

According to the previous sections, there are two spin-selective phases in the present non-local mixture model, so it is of great value to analyze how the phase diagram from Fig. 1 changes as we increase the spin population imbalance. This is depicted in Fig. 9, where we exhibit the phase diagram for $I \in \{0, 1/6, 1/2, 1\}$. Here, we ob-

serve that the phase space configuration of the mixed Mott (dark blue) and mixed CDW (brown) insulators is invariant under the change of the spin population imbalance, which further emphasizes its non-spin-selective nature. On the other hand, as we increase I , we can see the splitting of the spin-selective phases. In the case of the spin-selective Mott insulator (dark green) the separation grows until the spin-up insulator follows $\rho_B = 1$ while the other one matches the mixed Mott insulator. For the spin-selective CDW (light green), there is an additional constraint, $\rho_B + \rho_F \geq 1$; hence as the imbalance increases, the spin-down phase shortens until it vanishes at $I = 1$, while the spin-up phase follows the relation $\rho_B - \rho_F = 0$. In the case of the immiscible CDW (purple line), the condition $1/2 \leq \rho_F \leq 1/(1+I)$ limits its phase space line as I grows until it converges at the point $\rho_B = \rho_F = 1/2$. So for polarized fermions at half-filling the three different insulators found in this study follow the single condition $\rho_B - \rho_F = 0$. This emphasizes how a study with spinor fermions can in fact show different emergent behavior that can be elusive in an investigation with only scalar particles.

IV. CONCLUSIONS

In the present study, we have introduced three incommensurable insulators that emerge after taking into account next-neighbor fermionic interactions for a Bose-Fermi mixture model of two-color fermions and scalar bosons at the hardcore limit. We used an MPS-based DMRG method in order to obtain the ground state for given carrier densities and interaction parameters and subsequently constructed plots of the bosonic density against the bosonic chemical potential to determine the presence of the corresponding incompressible phases. We also constructed multiple density profiles and phase diagrams, varying the next-neighbor interaction between fermions for the purpose of characterizing the properties of the cited insulators.

First, and as a continuation of previous investigations like [27, 67–71], we analyzed how the mixed and spin-selective Mott insulators change with the addition of the next-neighbor fermionic interactions. Here we found that for $\rho_F < 1/2$, the mixed Mott insulator increases its stability by combining the commensurable and CDW orderings, while for $\rho_F \geq 1/2$, the insulator diminishes its charge gap until it vanishes at a critical next-neighbor interaction parameter, since in this case a commensurable order is incompatible with the CDW one. In general, the stability of the spin-selective phase decreases as we increase V_{FF} as an effect of the unpaired fermions in the system that can perturb the mutual structure of the bosons and paired fermions. Nevertheless, for $\rho_F < 1/2$ this decrease is damped by the compatibility of the commensurable ordering between paired fermions and bosons and the CDW ordering, which even leads to values of V_{FF} where the charge gap increases.

Now for $\rho_B = 1/2$, we found the immiscible CDW insulator, which has a charge density wave ordering for both fermions and bosons that are completely out of phase. It was established that this insulator only appears for $1/2 \leq \rho_F \leq 1/(1+I)$, which is associated with the system having just enough fermions to create the characteristic dimerized lattice from the CDW ordering. The gap from this incompressible phase grows with increasing next-neighbor fermion interaction, since this non-local repulsion provides stability to the CDW structure.

On the other hand, another non-trivial insulator appears for $\rho_B - \rho_F = 0$, where there are two CDW orderings present, a local one analogous to the immiscible CDW insulator and a global one that encloses the latter; hence we denote this a mixed CDW insulator. This phase only appears for $\rho_B + \rho_F \leq 1$, and we associate its emergence with the generation of Bose-Fermi composites that are distributed across the system and have an effective repulsive interaction, which gives rise to the incompressible nature of the phase. Because of this effective interaction, as we increase the non-local fermionic interaction and the stability, the gap of the mixed CDW insulator also increases.

Moreover, we also found a spin-selective analog to the previously mentioned insulator, which appears for $\rho_B - \rho_F^{\uparrow,(\downarrow)} = 0$, given that the total number of carriers is larger than the system size, that is $\rho_B + \rho_F \geq 1$. In this case, the plateau with higher bosonic density has the same structure as the mixed CDW insulator, while the other possesses an unclear structure. We associate this with the effect that the free fermions from the opposite spin have on the insulator structure, and because of that, after a certain value of the next-neighbor fermionic interaction as we increase the latter, the gap decreases until it vanishes.

Even though we have found these three incommensurable insulators, there are still open questions regarding their nature. As an example, one can wonder what happens when we remove the hard core approximation. In this case, we anticipate that the diagram from Fig. 1 should repeat as we consider higher bosonic densities. This has already been observed for the mixed and spin-selective insulators, where the relations that they follow change to $\rho_B + \rho_F = n$ and $\rho_B + \rho_F^{\uparrow,(\downarrow)} = n$, respectively, with n being an integer [69]. Either way, we do not discount the appearance of other insulators that could emerge from reducing the hard core restriction. Moreover, this study is focused on a particular set of values for the local interspecies and intraspecies interactions, but it is important to think of the effect that changing these parameters can have on these insulators. We observed that for $\rho_F = 4/5$, the stability of the spin-selective and immiscible CDW insulators increases for higher values of the local interspecies interaction U_{BF} , since this parameter modulates the mutual behavior between species that characterizes these CDW insulators. On the other hand, a small increase in the local fermionic interaction U_{FF} can lead to a charge gap increase in the immiscible CDW

phase, due to the localization of the fermions in the CDW ordering, and a decrease in the spin-selective CDW phase stability because of stronger perturbations caused by the free fermions in the insulator. However, a more thorough study has yet to be done.

Hence we trust that our investigation can inspire future research on the extended Bose-Fermi Hubbard model and specifically the previously shown incompressible phases, since their CDW character presents an opportunity to observe new emerging behavior in mixtures that could give rise to possible applications in industry [92]. So an experimental observation of these insulators would be a crucial input for the research on this topic. One novel option lies in the condensed matter systems, where it has been possible to create Bose-Fermi mixtures using solid-state superstructures from which fermionic and bosonic quasi-particles emerge that can at the same time inter-

act with each other [93]. On the other hand, the usual setup for these types of mixtures lies in the optical lattices field, where we believe that methods like the one proposed by [27] can assist with this task, since for example using heteronuclear photoassociation in a system set at the immiscible CDW phase should result in a null double interspecies and subsequently with absorption imaging, the characteristic dimerized structure of the phase could be determined. Consequently, we hope that there can be more advanced techniques proposed in modern cold-atom setups which can fulfill this task.

ACKNOWLEDGMENTS

Silva-Valencia acknowledges the support of the DIBB - Universidad Nacional de Colombia (Grant No. 51116).

[1] I. Bloch, J. Dalibard, and W. Zwerger, *Rev. Mod. Phys.* **80**, 885 (2008).

[2] T. Esslinger, *Annu. Rev. Condens. Matter Phys.* **1**, 129 (2010).

[3] I. Bloch, J. Dalibard, and S. Nascimbéne, *Nat. Phys.* **8**, 267 (2012).

[4] C. Gross and I. Bloch, *Science* **357**, 995 (2017).

[5] M. Greiner, O. Mandel, T. Esslinger, T. W. Hänsch, and I. Bloch, *Nature* **415**, 39 (2002).

[6] R. Jördens, N. Strohmaier, K. Günter, H. Moritz, and T. Esslinger, *Nature* **455**, 204 (2008).

[7] U. Schneider, L. Hackermüller, S. Will, T. Best, I. Bloch, T. A. Costi, R. W. Helmes, D. Rasch, and A. Rosch, *Science* **322**, 1520 (2008).

[8] W. S. Bakr, A. Peng, M. E. Tai, R. Ma, J. Simon, J. I. Gillen, S. Fölling, L. Pollet, and M. Greiner, *Science* **329**, 547 (2010).

[9] J. F. Sherson, C. Weitenberg, M. Endres, M. Cheneau, I. Bloch, and S. Kuhr, *Nature* **467**, 68 (2010).

[10] D. Greif, M. F. Parsons, A. Maziurenko, C. S. Chiu, S. Blatt, F. Huber, G. Ji, and M. Greiner, *Science* **351**, 953 (2016).

[11] A. F. Andreev and E. P. Bashkin, *Sov. Phys.-JETP* **42**, 164 (1975).

[12] G. E. Volovik, V. P. Mineev, and I. M. Khalatnikov, *Sov. Phys.-JETP* **42**, 342 (1975).

[13] A. G. Truscott, K. E. Strecker, W. I. McAlexander, G. B. Partridge, and R. G. Hulet, *Science* **291**, 2570 (2001).

[14] F. Schreck, L. Khaykovich, K. L. Corwin, G. Ferrari, T. Bourdel, J. Cubizolles, and C. Salomon, *Phys. Rev. Lett.* **87**, 080403 (2001).

[15] Z. Hadzibabic, C. A. Stan, K. Dieckmann, S. Gupta, M. W. Zwierlein, A. Görlitz, and W. Ketterle, *Phys. Rev. Lett.* **88**, 160401 (2002).

[16] G. Roati, F. Riboli, G. Modugno, and M. Inguscio, *Phys. Rev. Lett.* **89**, 150403 (2002).

[17] H. Ott, E. de Mirandes, F. Ferlaino, G. Roati, G. Modugno, and M. Inguscio, *Phys. Rev. Lett.* **92**, 160601 (2004).

[18] C. Silber, S. Günther, C. Marzok, B. Deh, P. W. Courteille, and C. Zimmermann, *Phys. Rev. Lett.* **95**, 170408 (2005).

[19] K. Günter, T. Stöferle, H. Moritz, M. Köhl, and T. Esslinger, *Phys. Rev. Lett.* **96**, 180402 (2006).

[20] S. Ospelkaus, C. Ospelkaus, O. Wille, M. Sacco, P. Ernst, K. Sengstock, and K. Bongs, *Phys. Rev. Lett.* **96**, 180403 (2006).

[21] M. Zaccanti, C. D'Errico, F. Ferlaino, G. Roati, M. Inguscio, and G. Modugno, *Phys. Rev. A* **74**, 041605(R) (2006).

[22] J. M. McNamara, T. Jeltes, A. S. Tychkov, W. Hogervorst, and W. Vassen, *Phys. Rev. Lett.* **97**, 080404 (2006).

[23] T. Best, S. Will, U. Schneider, L. Hackermüller, D. van Oosten, I. Bloch, and D.-S. Lühmann, *Phys. Rev. Lett.* **102**, 030408 (2009).

[24] T. Fukuhara, S. Sugawa, Y. Takasu, and Y. Takahashi, *Phys. Rev. A* **79**, 021601(R) (2009).

[25] B. Deh, W. Gunton, B. G. Klappauf, Z. Li, M. Semczuk, J. V. Dongen, and K. W. Madison, *Phys. Rev. A* **82**, 020701(R) (2010).

[26] M. K. Tey, S. Stellmer, R. Grimm, and F. Schreck, *Phys. Rev. A* **82**, 011608(R) (2010).

[27] S. Sugawa, K. Inaba, S. Taie, R. Yamazaki, M. Yamashita, and Y. Takahashi, *Nat. Phys.* **7**, 642 (2011).

[28] T. Schuster, R. Scelle, A. Trautmann, S. Knoop, M. K. Oberthaler, M. M. Haverhals, M. R. Goosen, S. J. J. M. F. Kokkelmans, and E. Tiemann, *Phys. Rev. A* **85**, 042721 (2012).

[29] S. K. Tung, C. Parker, J. Johansen, C. Chin, Y. Wang, and P. S. Julienne, *Phys. Rev. A* **87**, 010702(R) (2013).

[30] I. Ferrier-Barbut, M. Delehaye, S. Laurent, A. T. Grier, M. Pierce, B. S. Rem, F. Chevy, and C. Salomon, *Science* **345**, 1035 (2014).

[31] M. Delehaye, S. Laurent, I. Ferrier-Barbut, S. Jin, F. Chevy, and C. Salomon, *Phys. Rev. Lett.* **115**, 265303 (2015).

[32] V. D. Vaidya, J. Tiamsuphat, S. L. Rolston, and J. V. Porto, *Phys. Rev. A* **92**, 043604 (2015).

[33] X.-C. Yao, H.-Z. Chen, Y.-P. Wu, X.-P. Liu, X.-Q. Wang, X. Jiang, Y. Deng, Y.-A. Chen, and J.-W. Pan, *Phys. Rev. Lett.* **117**, 145301 (2016).

[34] R. Onofrio, *Phys. Usp.* **59**, 1129 (2016).

[35] Y.-P. Wu, X.-C. Yao, H.-Z. Chen, X.-P. Liu, X.-Q. Wang, Y.-A. Chen, and J.-W. Pan, *J. Phys. B: At. Mol. Opt. Phys.* **50**, 094001 (2017).

[36] R. Roy, A. Green, R. Bowler, and S. Gupta, *Phys. Rev. Lett.* **118**, 055301 (2017).

[37] F. Schäfer, N. Mizukami, P. Yu, S. Koibuchi, A. Bouscal, and Y. Takahashi, *Phys. Rev. A* **98**, 051602(R) (2018).

[38] R. S. Lous, I. Fritsche, M. Jag, F. Lehmann, E. Kirilov, B. Huang, and R. Grimm, *Phys. Rev. Lett.* **120**, 243403 (2018).

[39] A. Trautmann, P. Ilzhöfer, G. Durastante, C. Politi, M. Sohmen, M. J. Mark, and F. Ferlaino, *Phys. Rev. Lett.* **121**, 213601 (2018).

[40] B. J. DeSalvo, K. Patel, G. Cai, and C. Chin, *Nature* **568**, 61 (2019).

[41] A. Albus, F. Illuminate, and J. Eisert, *Phys. Rev. A* **68**, 023606 (2003).

[42] M. Cazalilla and A. Ho, *Phys. Rev. Lett.* **91**, 150403 (2003).

[43] M. Lewenstein, L. Santos, M. A. Baranov, and H. Fehrmann, *Phys. Rev. Lett.* **92**, 050401 (2004).

[44] L. Mathey, D.-W. Wang, W. Hofstetter, M. D. Lukin, and E. Demler, *Phys. Rev. Lett.* **93**, 120404 (2004).

[45] R. Roth and K. Burnett, *Phys. Rev. A* **69**, 021601 (2004).

[46] H. Frahm and G. Palacios, *Phys. Rev. A* **72**, 061604 (2005).

[47] M. T. Batchelor, M. Bortz, X. W. Guan, and N. Oelkers, *Phys. Rev. A* **72**, 061603 (2005).

[48] Y. Takeuchi and H. Mori, *Phys. Rev. A* **72**, 063617 (2005).

[49] L. Pollet, M. Troyer, K. V. Houcke, and S. Rombouts, *Phys. Rev. Lett.* **96**, 190402 (2006).

[50] L. Mathey and D.-W. Wang, *Phys. Rev. A* **75**, 013612 (2007).

[51] K. Sengupta, N. Dupuis, and P. Majumdar, *Phys. Rev. A* **75**, 063625 (2007).

[52] A. Mering and M. Fleischhauer, *Phys. Rev. A* **77**, 023601 (2008).

[53] K. Suzuki, T. Miyakawa, and T. Suzuki, *Phys. Rev. A* **77**, 043629 (2008).

[54] D.-S. Lühmann, K. Bongs, K. Sengstock, and D. Pfannkuche, *Phys. Rev. Lett.* **101**, 050402 (2008).

[55] M. Rizzi and A. Imambeikov, *Phys. Rev. A* **77**, 023621 (2008).

[56] P. P. Orth, D. L. Bergman, and K. L. Hur, *Phys. Rev. A* **80**, 023624 (2009).

[57] X. Yin, S. Chen, and Y. Zhang, *Phys. Rev. A* **79**, 053604 (2009).

[58] S. Sinha and K. Sengupta, *Phys. Rev. B* **79**, 115124 (2009).

[59] E. Originac, M. Tsuchizawa, and Y. Suzumura, *Phys. Rev. A* **81**, 053626 (2010).

[60] T. P. Polak and T. K. Kopeć, *Phys. Rev. A* **81**, 043612 (2010).

[61] A. Mering and M. Fleischhauer, *Phys. Rev. A* **81**, 011603(R) (2010).

[62] P. Anders, P. Werner, M. Troyer, M. Sigrist, and L. Pollet, *Phys. Rev. Lett.* **109**, 206401 (2012).

[63] A. Masaki and H. Mori, *J. Phys. Soc. Jpn.* **82**, 074002 (2013).

[64] M. Bukov and L. Pollet, *Phys. Rev. B* **89**, 094502 (2014).

[65] T. Ozawa, A. Recati, M. Delehaye, F. Chevy, and S. Stringari, *Phys. Rev. A* **90**, 043608 (2014).

[66] T. Bilitewski and L. Pollet, *Phys. Rev. B* **92**, 184505 (2015).

[67] A. Zujev, A. Baldwin, R. T. Scalettar, V. G. Rousseau, P. J. H. Denteneer, and M. Rigol, *Phys. Rev. A* **78**, 033619 (2008).

[68] R. Avella, J. J. Mendoza-Arenas, R. Franco, and J. Silva-Valencia, *Phys. Rev. A* **100**, 063620 (2019).

[69] R. Avella, J. J. Mendoza-Arenas, R. Franco, and J. Silva-Valencia, *Phys. Rev. A* **102**, 033341 (2020).

[70] R. Guerrero-Suarez, J. J. Mendoza-Arenas, R. Franco, and J. Silva-Valencia, *Phys. Rev. A* **103**, 023304 (2021).

[71] J. Silva-Valencia, *Rev. Acad. Colomb. Cienc. Exactas Fis. Nat.* **46**, 877 (2022).

[72] B. M. Spar, E. Guardado-Sánchez, S. Chi, Z. Z. Yan, and W. S. Bakr, *Physical Review X* **11**, 021036 (2021).

[73] X. Wang, E. Khatami, F. Fei, J. Wyrick, P. Namboodiri, R. Kashid, A. F. Rigos, G. Bryant, and R. Silver, *Nat. Commun.* **13**, 6824 (2022).

[74] T. D. Kühner, S. R. White, and H. Monien, *Phys. Rev. B* **61**, 12474 (2000).

[75] R. V. Pai and R. Pandit, *Phys. Rev. B* **71**, 104508 (2005).

[76] G. G. Batrouni, F. Hebert, and R. T. Scalettar, *Phys. Rev. Lett.* **97**, 087209 (2006).

[77] T. Mishra, R. V. Pai, S. Ramanan, M. S. Luthra, and B. P. Das, *Phys. Rev. A* **80**, 043614 (2009).

[78] D. Rossini and R. Fazio, *New J. Phys.* **14**, 065012 (2012).

[79] R. T. Clay, A. W. Sandvik, and D. K. Campbell, *Phys. Rev. B* **59**, 4655 (1999).

[80] S. Ejima and S. Nishimoto, *Phys. Rev. Lett.* **99**, 216403 (2007).

[81] M. Nakamura, *Phys. Rev. B* **61**, 16377 (2000).

[82] E. Jeckelmann, *Phys. Rev. Lett.* **89**, 236401 (2002).

[83] A. W. Sandvik, L. Balents, and D. K. Campbell, *Phys. Rev. Lett.* **92**, 236401 (2004).

[84] S.-S. Deng, S.-J. Gu, and H.-Q. Lin, *Phys. Rev. B* **74**, 045103 (2006).

[85] F. Iemini, T. O. Maciel, and R. O. Vianna, *Phys. Rev. B* **92**, 075423 (2015).

[86] J. J. Mendoza-Arenas, *J. Stat. Mech.* **2022**, 043101 (2022).

[87] B. Wang, D.-W. Wang, and S. Das Sarma, *Phys. Rev. A* **82**, 021602 (2010).

[88] T. Ikemachi, A. Ito, Y. Aratake, Y. Chen, M. Koashi, M. Kuwata-Gonokami, and M. Horikoshi, *J. Phys. B: At. Mol. Opt. Phys.* **50**, 01LT01 (2017).

[89] Y. Takasu and Y. Takahashi, *J. Phys. Soc. Jpn.* **78**, 012001 (2009).

[90] U. Schollwöck, *Ann. Phys.* **326**, 96 (2011).

[91] J. Hauschild and F. Pollmann, *SciPost Phys. Lect. Notes*, 5 (2018).

[92] A. A. Balandin, S. V. Zaitsev-Zotov, and G. Grüner, *Appl. Phys. Lett.* **119**, 170401 (2021).

[93] D. A. Ruiz-Tijerina, *Nat. Mater.* **22**, 153 (2023).